JBMR Plus, 2025, **9**, ziaf058
https://doi.org/10.1093/jbmrpl/ziaf058
Advance access publication: April 9, 2025
Research Article

Osseous morphology differences in the foot and ankle associated with Charcot-Marie-Tooth disease

Melissa R. Requist[1,2], Andrew C. Peterson[1], Timothy C. Beals[3], Bopha Chrea[4], Amy L. Lenz[1,2,5,*]

[1]Department of Mechanical Engineering, University of Utah, Salt Lake City, UT 84112, United States
[2]Department of Biomedical Engineering, University of Utah, Salt Lake City, UT 84112, United States
[3]The Orthopedic Partners, Park City, UT 84060, United States
[4]Department of Orthopaedics and Rehabilitation, University of Iowa, Iowa City, IA 52242, United States
[5]Department of Orthopaedics, University of Utah, Salt Lake City, UT 84108, United States
*Corresponding author: Amy L. Lenz, Department of Mechanical Engineering, University of Utah, 1495 S 100 E, Salt Lake City, UT 84112, United States (amy.lenz@utah.edu)

Abstract

Charcot-Marie-Tooth (CMT) disease is a genetic, progressive peripheral nerve disease that commonly manifests in a cavovarus foot deformity. Previously, this foot deformity has been believed to be an alignment change in the foot, but recent research has shown that there are bone morphology differences in individuals with CMT. Differences in bone morphology have been identified in the calcaneus, talus, and medial cuneiform, but have not been consistently analyzed throughout the foot or studied in relation to different genetic subtypes of CMT. This study is a retrospective, cross-sectional analysis of bone morphology in CMT using weight-bearing computed tomography and statistical shape modeling. This analysis identified bone morphology differences between CMT and control groups throughout the hindfoot, midfoot, and forefoot. Bone morphology differences were also present between the 2 primary disease subtypes throughout the foot. Key morphologic findings include the altered shape of the subtalar articular surfaces on the talus, bending of the metatarsals, variation in navicular process morphology, and differences between subtypes in the talus, medial cuneiform, and medial metatarsals. There are several possible theoretical mechanisms for this osseous deformation, including bone remodeling in response to altered loading from alignment change or from decreased musculotendinous forces, but the patterns of morphological variation seen in these data cannot be fully explained by these mechanisms, suggesting that there may be an interaction between the neuronal disease and bone remodeling. Future work is necessary to characterize the progression of bony deformity throughout development and to correlate bone shape with function, gait, muscle morphology and strength to elucidate the mechanism of osseous morphology change in varying subtypes of CMT.

Keywords: Charcot-Marie-Tooth disease, Statistical Shape Modeling, Bone morphology, Foot and Ankle, Weight-bearing CT, cavovarus deformity

Lay Summary

Charcot-Marie-Tooth (CMT) disease is a neurologic disease that is associated with a characteristic foot deformity. Current understanding of CMT suggests that this deformity is caused by malalignment in the foot, but recent research has identified shape changes in individual bones in people with this disease. This study used computational modeling from medical images to analyze bone shape between individuals with 2 primary subtypes of CMT and a control group. The bone shape differences identified throughout the foot support multiple potential theories of bone shape change and are relevant in understanding the foot complications and progression of this disease.

Received: December 9, 2024. **Revised:** March 21, 2025. **Accepted:** April 2, 2025

Graphical Abstract

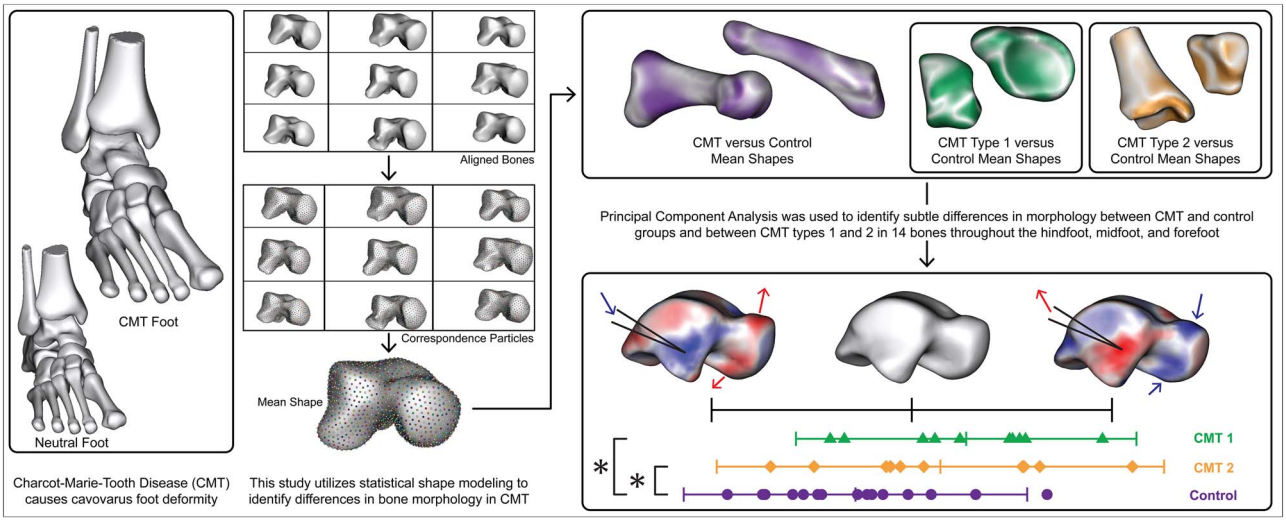

Introduction

Charcot-Marie-Tooth (CMT) disease is a rare progressive disease of peripheral nerves that most commonly presents with deformity and pain in the feet.[1–4] While there are a variety of foot complications associated with CMT, the most common is a cavovarus deformity, consisting of a high arch and varus hindfoot alignment.[1–3] The classical theory of deformity in CMT hypothesizes that alterations in foot shape are a result of alignment change due to altered muscle activation. However, recent work suggests that changes in bony morphology may also contribute to this deformity.[5–7] Both the mechanism of this osseous deformity and the variability in alignment and morphologic deformity between subtypes of CMT are poorly understood.[2,8–11] Broadly, individuals with CMT show a greater occurrence of osteoporosis as well as deterioration in tibia microstructure versus age-matched controls, suggesting an interaction between this disease and overall bone health.[6] Specific differences in hindfoot bone shape have also been identified in CMT. Differences in calcaneus morphology consisting of a decreased calcaneal radius of curvature and decreased posterior tuberosity-posterior facet angle in the sagittal plane have been identified in CMT.[5] In the medial cuneiform, the bone shape differs such that the first tarsometatarsal joint is more plantarflexed relative to the anatomic axis of the bone in the CMT population than in controls.[12] Talus morphology is also substantially altered in CMT to have a flatter shape to the bone and a decrease in talar neck declination as compared to controls.[5,7] Between subtypes of CMT, a greater alteration of talar neck morphology was seen in CMT1 than CMT2.[7] Minimal work beyond this study has been done to characterize differences between subtypes of CMT, although CMT1 is believed to have a more severe deformity than CMT2 and higher occurrence of cavovarus foot deformity is seen in individuals with CMT1A.[2]

Statistical shape modeling (SSM) is a tool that is used to analyze morphologic and alignment variability throughout a population and is frequently used to describe variations in bony anatomy.[13–18] SSM from WBCT has been utilized in several foot and ankle structures, such as the talocrural, tibiofibular, subtalar, talonavicular, and calcaneocuboid joints, and in pathologies, such as osteoarthritis and flatfoot.[14–16,19–24] SSM has been used to study the talus in individuals with CMT, but has not yet been used to simultaneously model hindfoot, midfoot, and forefoot bones to examine the contribution of alignment and bony morphology to this deformity throughout the foot.[7] Identifying the locations of bony morphology change relative to tendinous and ligamentous attachments, articular surfaces, and patterns of load distribution across the foot provides valuable insight to develop a theory for the interaction between known neurologic pathophysiology and alterations in bone structure. The complicated interactions between muscle innervation loss, alterations in loading and in musculotendinous forces acting on bone, and the neurologic factors that impact bone metabolism are poorly understood.[25–28] While CMT1 is typically characterized as a more severe deformity, the talar morphology differences identified between subtypes suggest that there may be different patterns of bone morphology adaptation in specific subtypes of CMT. Additionally, a difference in severity or deformity pattern between types may obscure bony differences between either type or controls due to the heterogeneity in a combined CMT population. This study aims to use SSM to analyze differences in individual bone morphology in the hindfoot, midfoot, and forefoot in individuals with CMT and to conduct an exploratory analysis of bone morphology differences between CMT types 1 and 2. This improved understanding of foot bone structure will aid in understanding the pathophysiology of the disease and developing improved treatment algorithms.

Materials and methods

Twenty-nine WBCT scans from 19 individuals with CMT and a cavovarus foot type seen at either the University of Utah or the University of Iowa were retrospectively identified, representing both unilateral and bilateral WBCT scans (Table 1). Individuals with a prior surgical history on the included limb were excluded in order to better study the natural history of the disease. Additionally, individuals with comorbid Charcot arthropathy were excluded. Fifteen control WBCT scans were identified as contralateral limbs from individuals who received bilateral WBCT for an acute unilateral Lisfranc injury with the same exclusion criteria as the CMT

Table 1. Demographics and genetic subtype for WBCT scans of individuals with CMT and controls.

	Individuals	Limbs	Sex	Age (range)	BMI (range)
CMT	19	29	12 F, 17 M	44.4 (13–75)	31.2 (18.0–46.7)
CMT1	7	10	4 F, 6 M	40.9 (18–71)	26.4 (23.1–26.5)
CMT2	7	10	5 F, 5 M	41.6 (14–70)	36.3 (29.0–46.7)
Control	15	15	6F, 9 M	39.7 (17–69)	26.7 (20.8–39.2)

group. Individuals with CMT were separated by subtype diagnosis into a group of CMT type 1 (CMT1) and CMT type 2 (CMT2) by genetic or electromyography diagnosis. Individuals with other subtypes, including CMTX and CMT4, were not included in subtype analysis. This categorization yielded 10 CMT1 and 10 CMT2 limbs (Table 1).

WBCT scans were collected using a pedCAT (CurveBeam LLC, 0.37mm^3 voxel size, kVp 120, mAs 22-62). Following an established protocol, the tibia through metatarsal were segmented from WBCT images semi-automatically (Bonelogic, DISIOR, Paragon 28) with manual verification (Mimics, Materialise). The 3D bone structures generated by each segmentation were consistently smoothed and decimated (3-Matic, Materialise) then aligned using an iterative closest point alignment algorithm. In this alignment, all left-sided images were mirrored across the sagittal plane to appear as right feet for the analysis. Additionally, the tibia and fibula were consistently cropped 65 mm proximal to the tibiotalar articular surface for consistency in modeling. Statistical shape models were generated for each of the 14-bones (Shapeworks, Scientific Computing and Imaging Institute). A generalized Procrustes analysis was used during SSM generation to remove the effect of size variation from the results.[29,30]

Statistical analysis

Differences in age, BMI, and Procrustes scale factor between CMT and control groups were tested with Student's *t*-tests with significance level $\alpha = .05$. Differences in age, BMI, and Procrustes scale factor between CMT1, CMT2, and control groups were tested with a single factor ANOVA. Differences in sex distribution between CMT and control groups and between CMT1, CMT2, and control groups were tested with a chi squared test. Following methodology previously published for bony morphology analysis in other foot and ankle pathologies, principal component analysis (PCA) was used to identify specific modes of variation in each bone that represent a portion of the shape variance in the population.[14,15,17,21,31–33] Parallel analysis, which compares the proportion of variance represented by a PCA mode to the proportion represented by the equivalent mode in simulated random data, was used to determine modes that represented a more than random portion of variance, which are referred to as significant modes in the remainder of this analysis.[13,34] To compare PCA component scores between groups along each mode, non-parametric tests were used due to the combination of bilateral and unilateral data. These tests were a Wilcoxon rank sum test with Holm–Sidak correction for differences between CMT and control groups and a Kruskal–Wallace test with Dunn–Sidak post-hoc analysis for differences between CMT1, CMT2, and control groups.[23] All statistical tests used a significance value of $\alpha = .05$. Hedge's g effect size was calculated for comparisons between CMT and control groups along each significant mode of variation.

Results

There was no significant difference ($p = .52$) in age at scan or in BMI between the CMT and control groups or between the CMT1, CMT2, and control groups ($p = .968$). There was no difference in age at diagnosis between the CMT1 and CMT2 groups ($p = .4$). However, there were differences in BMI between groups ($p < .001$), with the CMT2 group having a higher BMI than the CMT1 or control groups. There was no difference in sex distribution between CMT and control groups ($p = .93$) or between CMT1, CMT2, or control groups ($p = .864$). Differences between sexes were not analyzed because, when split by sex, the male CMT group had a significantly higher age than the female CMT group ($p < .001$), so a larger, more diverse dataset is necessary to study the impact of sex without this confounding factor. The average Procrustes scale factor did not differ between CMT and control groups ($p = .238$) or between CMT1, CMT2, and control groups ($p = .614$). Procrustes scale factors ranged from 0.887 to 1.145. Hedges' g effect size was calculated for differences between CMT and control groups along each significant mode of variation for all 14 bones and corrected for the small sample size (Table SA-4).[35,36] This yielded a large average effect size for the comparisons that showed a significant difference between modes ($g = 1.096$) and a small average effect size when looking at all modes regardless of difference between CMT and control groups ($g = 0.410$).

Significant differences between CMT and control groups were identified along at least one PCA mode in the full foot and in 11 out of the 14 single bones. Significant differences between CMT1, CMT2, and control groups were identified along at least one PCA mode in all 14 bones, with differences between CMT1 and control in 13 bones, CMT2 and control in 8 bones, and differences between CMT1 and CMT 2 in 9 bones. An overview of these results is given in Table 2.

In the ankle and hindfoot, differences between CMT and control groups were identified in the tibia and talus (Figure 1). *p*-values for all PCA component score tests in this region are given in Table SA-1. The third mode of variation in the tibia (Figure 1A) represented a difference in the length of the medial malleolus and depth of the fibular notch, with the control distribution toward the negative direction, indicative of a shorter medial malleolus and shallower fibular notch, and the CMT distribution toward the positive direction, indicative of a longer medial malleolus and deeper fibular notch.[37] There was a significant difference along this mode in the tibia between CMT and control groups ($p = .009$). This same difference was identified between the CMT2 and control groups ($p = .018$), but not between CMT1 and control groups. The eighth mode

Table 2. Summary of PCA results identifying group comparisons with a significant difference in at least one mode of variation for comparisons between CMT and control groups and between CMT1, CMT2, and control groups.

Model	CMT vs Control	CMT1 vs Control	CMT2 vs Control	CMT1 vs CMT2
Tibia	X		X	
Fibula		X		X
Talus	X	X	X	X
Calcaneus		X		
Navicular	X	X		X
Cuboid	X	X	X	
Medial cuneiform	X	X	X	X
Intermediate cuneiform	X	X		X
Lateral cuneiform		X	X	X
Metatarsal 1	X	X		X
Metatarsal 2	X	X		X
Metatarsal 3	X	X	X	X
Metatarsal 4	X	X	X	
Metatarsal 5	X	X	X	

of variation of the talus (Figure 1F) represented a flatter and wider posterior articular facet in the CMT group compared to controls ($p = .003$). This same talar morphology difference was seen between the CMT1 and control groups ($p = .012$). The ninth mode of variation in the talus (Figure 1G) demonstrated a medial shift of the talar neck relative to the talar body in CMT as compared to control ($p = .013$). Differences along this mode were also present between the CMT1 and control groups and CMT2 and control groups ($p = .024$, $p = .010$), where both subtypes showed the same medial shift of the talar neck as the overall CMT group, but the CMT2 group had a much wider distribution of shape scores.

Additional differences in this region of the foot were identified between CMT1, CMT2, and control groups in the fibula, calcaneus, and talus (Figure 1). p-values for all post-hoc PCA component score tests in the ankle and hindfoot are given in Table SB-1. In the fibula, the second mode of variation (Figure 1B) showed a significant difference between CMT1 and control groups ($p < .001$). This mode is representative of a decreased prominence of the posterior-medial ridge that serves as the attachment site for the deep transverse fascia of the leg in the CMT1 group as compared to both control and CMT2 groups. The third mode of variation in the calcaneus (Figure 1C) illustrates a reduced lateral prominence of the posterior facet and a thickening of the sustentaculum tali in the CMT1 group compared to controls ($p = .049$). The first mode of variation in the talus (Figure 1D) demonstrated a marked flattening of the medial and lateral borders of the trochlear surface accompanied by convexity of the superior-medial talar neck in the CMT1 group compared to taller trochlear surface borders and a mildly concave superior-medial talar neck in the controls ($p = .043$). The sixth mode of variation in the talus (Figure 1E) identified a medial prominence in the superior talar neck with associated concavity of the superior-lateral talar neck in the CMT2 group as compared to a more neutral medial neck and convex mid to lateral superior talar neck in the CMT1 group ($p = .005$) with the control group distributed central to the two subtypes.

In the midfoot, differences between CMT and control groups were identified in the navicular, cuboid, medial cuneiform, and intermediate cuneiform (Figures 2 and 3). p-values for all PCA component score tests in the midfoot are given in Table SA-2. The third mode of variation in the navicular (Figure 2A) demonstrated variability on the length of the navicular tuberosity, convexity or concavity of the inferior-medial region inferior to the navicular tuberosity, and height and distal projection of the naviculocuneiform articular surface. The +2 SD shape had a longer navicular tuberosity, concave inferior-medial surface, taller distal surface, and decreased distal projection of the articular surface. Contrarily, the −2 SD shape had a shorter navicular tuberosity, convex inferior-medial surface, and a shorter distal surface with increased distal projection of the naviculocuneiform articular surface. The control group distribution averages a positive value and ranges from just below the mean shape to just below +2 SDs, while the CMT group had a significantly different distribution that ranges from +2 to −2 SDs ($p = .015$). Differences along this mode in the same directions was also seen between the CMT1 and control groups and CMT1 and CMT2 groups ($p = .001$, $p = .030$) where the CMT1 group had a shorter tuberosity and more convex inferior-medial surface than either the control or CMT2 groups. In the cuboid, there is a significant difference between CMT and control groups in the seventh mode of variation ($p = .044$) (Figure 2D). This same difference was identified between the CMT2 and control groups ($p = .014$). This mode primarily demonstrated variability in the medial-lateral width of the distal articular surface, with the control distribution closer to the narrower articular surface and the CMT group and CMT2 group distributions closer to the wider articular surface. The first mode of variation in the medial cuneiform (Figure 3A) describes variation in the medial-lateral width of the plantar half of the bone along with an altered shape of the superior crest and shows a significant difference between CMT and control groups and between CMT1 and control groups ($p = .015$, $p = .001$). The CMT group and CMT1 group demonstrate a narrower medial-lateral width of the plantar cuneiform and increased height of the proximal side of the superior crest than seen in the control group. The intermediate cuneiform showed a difference between CMT and control groups, CMT1 and control groups, and CMT1 and CMT2 groups along the third mode of variation (Figure 3C) ($p = .030$, $p = .012$, $p = .001$). This mode of variation describes a medial-lateral shift of the dorsal surface of the bone relative to the center of the proximal and distal articular surfaces with a more lateral position of the

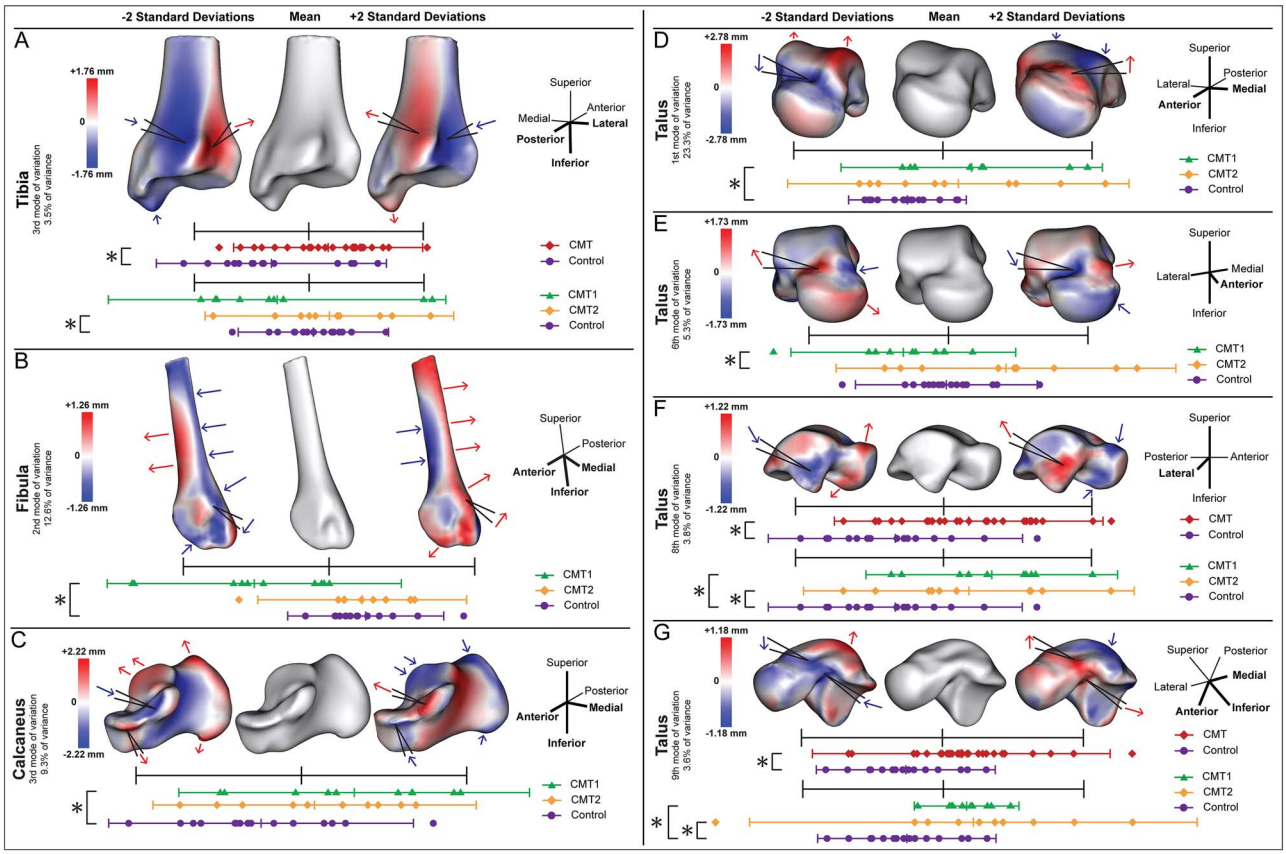

Figure 1. PCA modes in the ankle and hindfoot had a significant difference between CMT and control groups and/or between CMT1, CMT2, and control groups. These consist of (A) the third mode of variation in the tibia, (B) the second mode of variation in the fibula, (C) the third mode of variation in the calcaneus, (D) the first mode of variation in the talus, (E) the sixth mode of variation in the talus, (F) the eighth mode of variation in the talus, and (G) the ninth mode of variation in the talus. Red indicates a positive distance from the mean shape and blue indicates a negative distance from the mean shape. Distributions of the CMT and control groups and each of the subtype and control groups are shown underneath the images of the mean, positive 2 SD, and negative 2 SD shapes. Distributions not shown did not have any significant differences between their respective groups.

dorsal surface in the CMT1 group than the control or CMT2 groups.

Additional differences in the midfoot between the CMT1, CMT2, and control groups that were not seen between the CMT and control groups were identified in all bones of the midfoot (Figures 2 and 3). *p*-values for all post-hoc PCA component score tests in the midfoot are given in Table SB-2. In the navicular, the fourth mode of variation (Figure 2B) showed a significant difference between CMT1 and control groups ($p = .007$). This mode illustrated a decrease in the depth of the proximal side of the navicular tuberosity and an increased prominence on the inferior-medial navicular at the attachment site of the tibialis posterior tendon in the CMT1 group. The second mode of variation in the cuboid (Figure 2C) identified a shortening in the proximal-distal direction and increased superior-inferior height in CMT1 compared to the control group ($p = .012$). The third mode of variation in the medial cuneiform (Figure 3B) showed a difference between CMT1 and CMT2 subtypes, and between CMT1 and control groups ($p = .001$, $p = .012$). This mode represented a decreased plantar-proximal prominence in the CMT1 group versus and increased plantar-proximal prominence in the CMT2 group as well as an increased proximal-distal length in the CMT1 group as compared to the CMT2 and control groups. The fourth mode of variation in the intermediate cuneiform (Figure 3D) demonstrated a difference between the CMT2 and control groups ($p = .007$), where the CMT2 group had an increased superior-inferior height and decreased medial-lateral and proximal-distal thickness than the control group. The fifth mode of variation in the intermediate cuneiform (Figure 3E) identified a difference between CMT1 and CMT2 ($p = .038$), where the CMT1 group showed a proximal-lateral twist of the lateral articular surface compared to the CMT2 group. The third mode of variation in the lateral cuneiform (Figure 3F) demonstrated an increased plantar prominence and narrowing along the distal-proximal direction in the CMT2 group compared to controls ($p = .049$), with the CMT1 group trending in the same direction. The eighth mode of variation in the lateral cuneiform (Figure 3G) similarly depicts an in the distal-proximal direction with a slight decrease in plantar prominence in the CMT1 group as compared to the control and CMT2 groups ($p = .042$, $p = .001$).

Significant differences between CMT and control groups were seen along at least one PCA mode in all 5 metatarsals (Figures 4 and 5). *p*-values for all PCA component score tests in the forefoot are given in Table SA-3. In the first metatarsal, there was a significant difference between groups along the second mode of variation (Figure 4B) ($p = .002$). The CMT group demonstrated decreased plantar protrusion of the bone at the plantar-lateral metatarsal head, which is the attachment site for the peroneus longus tendon, as well as at the planar aspect of the metatarsal base on the tarsometatarsal articular

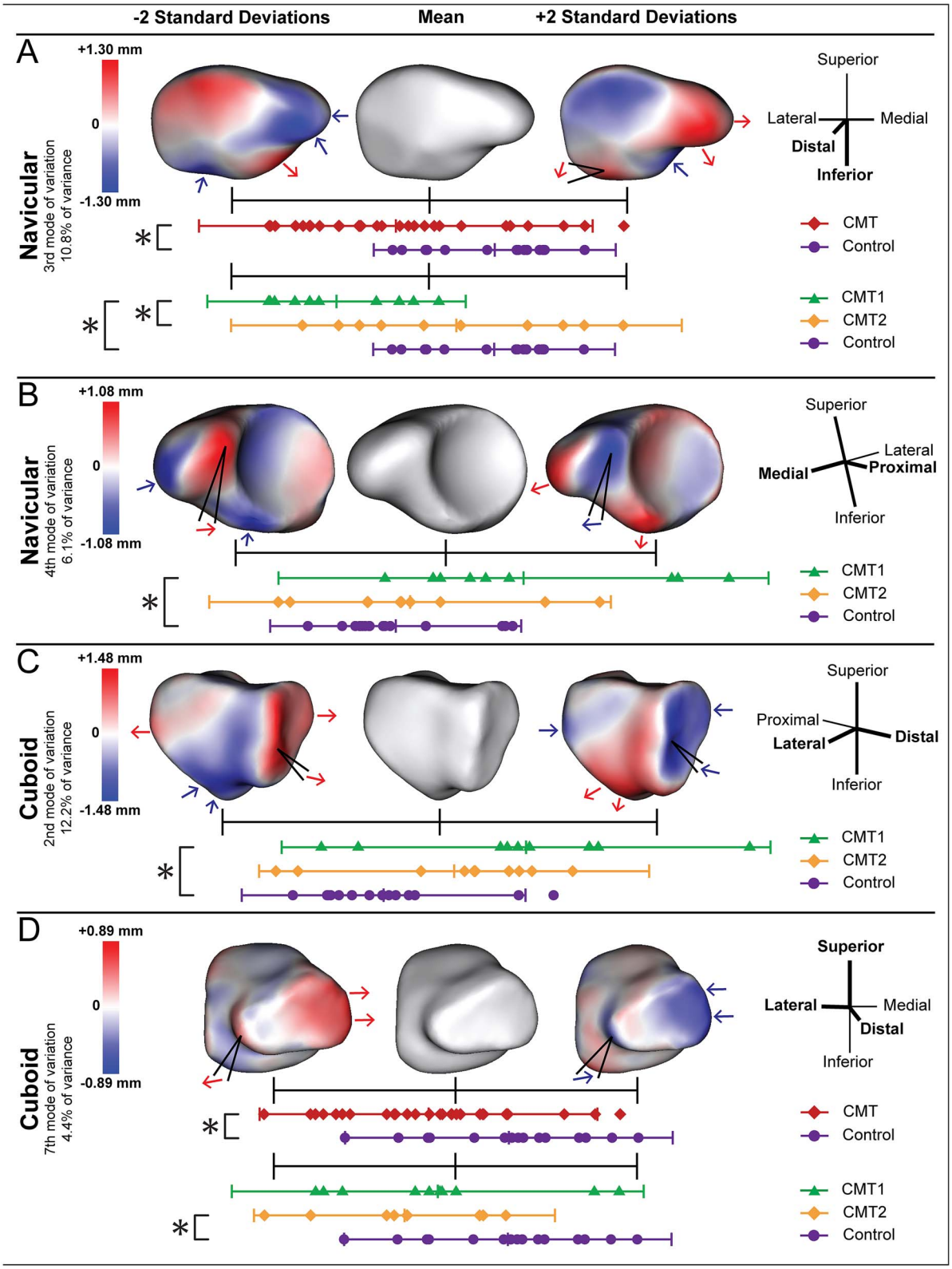

Figure 2. PCA modes in the proximal midfoot had a significant difference between CMT and control groups and/or between CMT1, CMT2, and control groups. These consist of (A) the third mode of variation in the navicular, (B) the fourth mode of variation in the navicular, (C) the second mode of variation in the cuboid, and (D) the seventh mode of variation in the cuboid. Red indicates a positive distance from the mean shape and blue indicates a negative distance from the mean shape. Distributions of the CMT and control groups and each of the subtype and control groups are shown underneath the images of the mean, positive 2 SD, and negative 2 SD shapes. Distributions not shown did not have any significant differences between their respective groups.

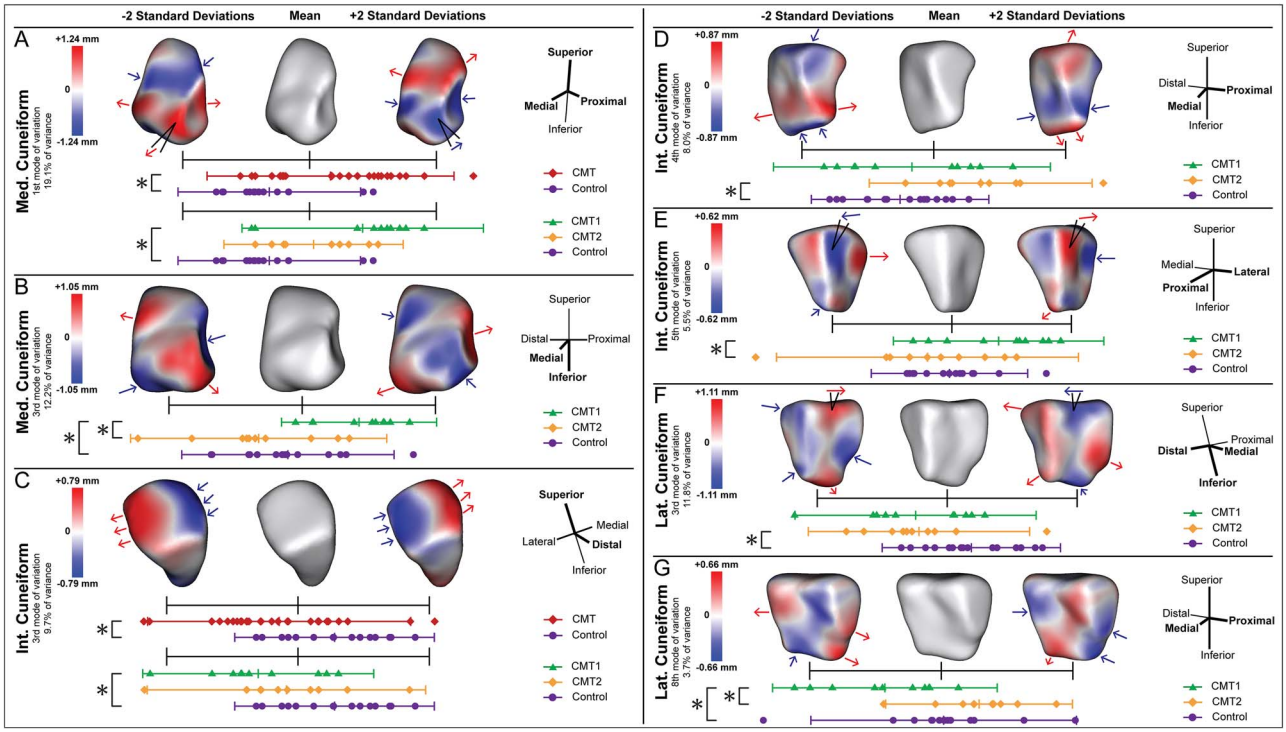

Figure 3. PCA modes in the distal midfoot had a significant difference between CMT and control groups and/or between CMT1, CMT2, and control groups. These consist of (A) the first mode of variation in the medial cuneiform, (B) the third mode of variation in the medial cuneiform, (C) the third mode of variation in the intermediate cuneiform, (D) the fourth mode of variation in the intermediate cuneiform, (E) the fifth mode of variation in the intermediate cuneiform, (F) the third mode of variation in the lateral cuneiform, and (G) the eighth mode of variation in the lateral cuneiform. Red indicates a positive distance from the mean shape and blue indicates a negative distance from the mean shape. Distributions of the CMT and control groups and each of the subtype and control groups are shown underneath the images of the mean, positive 2 SD, and negative 2 SD shapes. Distributions not shown did not have any significant differences between their respective groups.

surface. Concomitant morphologic variation at the proximal shaft of the metatarsal indicates a mild bending of the first metatarsal in the sagittal plane that is more aligned with the control group, with less bending in the CMT group. A significant difference along this mode was also identified between the CMT1 group and both the control and CMT2 groups ($p < .001$, $p = .040$). The CMT1 group demonstrated increased curvature with decreased proximal plantar protrusion than either the control or CMT2 groups. In the second metatarsal, the fourth modes of variation (Figure 4E) showed a significant difference between CMT and control groups ($p = .033$) with the CMT group demonstrating metatarsal bending in the axial plane with decreased lateral prominences of the metatarsal head and base and increased lateral arching of the shaft. This same difference was identified between the CMT1 and control groups ($p = .027$). The third mode of variation in the third metatarsal (Figure 5B) demonstrated sagittal plane bending of the metatarsal shaft, with a more plantar shaft position in the CMT group, as well as decreased medial extension of the distal articular surface at the metatarsal head and increased plantar prominence of the proximal articular surface at the metatarsal base in the CMT group compared to controls ($p < .001$). In the subtype analysis, both the CMT1 and CMT2 groups demonstrated this same morphologic difference from controls ($p = .001$, $p = .009$). The fourth metatarsal showed a difference between CMT and control groups along the fifth mode of variation (Figure 5E), which demonstrated decreased plantar prominence of the metatarsal head and increased plantar prominence of the metatarsal base in the CMT group ($p = .001$). Similar variation along this mode was also seen between the CMT2 and control groups ($p = .013$). The fourth mode of variation in the fifth metatarsal (Figure 5G) illustrated bowing of the metatarsal in the sagittal plane where there is bending of the shaft in the superior direction in the CMT group compared to a more neutral shaft orientation in the control group ($p = .003$). Both the CMT1 and CMT2 groups had this increased bowing of the fifth metatarsal compared to the control group ($p = .010$, $p = .001$).

Additional differences in the metatarsals between the CMT1, CMT2, and control groups that were not evident between CMT and control groups were seen in all 5 metatarsals (Figures 4 and 5). p-values for all post-hoc PCA component score tests in the forefoot are given in Table SB-3. The first mode of variation in the first metatarsal (Figure 4A) illustrated a shorter and thicker first metatarsal in CMT1 as compared to both CMT2 and control groups ($p = .036$, $p = .043$). The first mode of variation in the second metatarsal (Figure 4C) illustrated additional bending of the second metatarsal in an oblique plantar-medial to dorsal-lateral plane with a simultaneous difference in metatarsal head size. This mode demonstrated a difference between the CMT1 group and both the CMT2 and control groups ($p = .021$, $p = .001$). The CMT2 group demonstrated decreased bending and a smaller metatarsal head, while the CMT1 group had a larger head relative to shaft diameter and increased bending. The third mode of variation in the second metatarsal (Figure 4D) illustrated bending in the sagittal plane, with a more dorsal position of the metatarsal head and base and plantar position of the shaft in the CMT1 group compared to

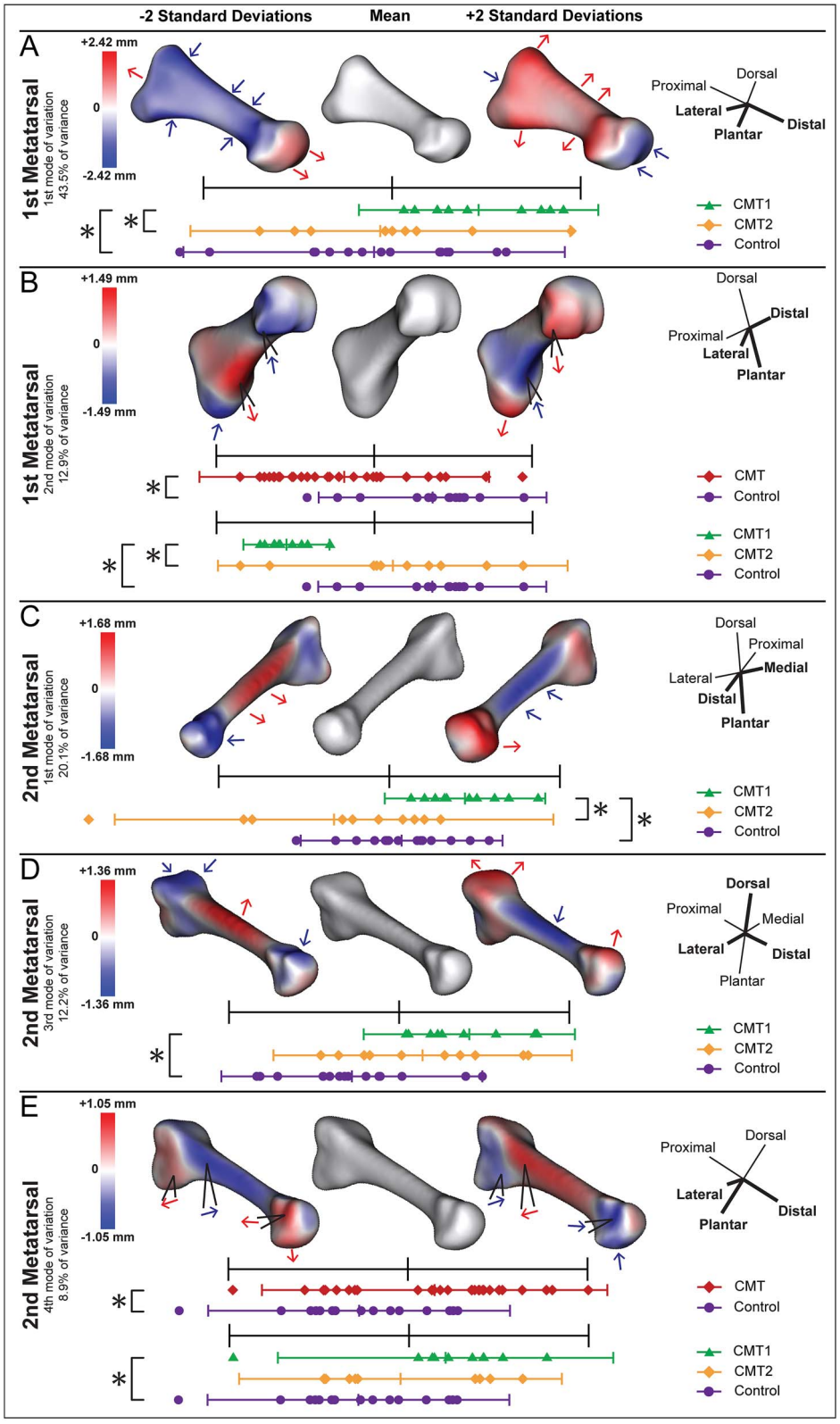

Figure 4. PCA modes in the medial forefoot had a significant difference between CMT and control groups and/or between CMT1, CMT2, and control groups. These consist of (A) the first mode of variation in the first metatarsal, (B) the second mode of variation in the first metatarsal, (C) the first mode of variation in the second metatarsal, (D) the third mode of variation in the second metatarsal, and (E) the fourth mode of variation in the second metatarsal. Red indicates a positive distance from the mean shape and blue indicates a negative distance from the mean shape. Distributions of the CMT and control groups and each of the subtype and control groups are shown underneath the images of the mean, positive 2 SD, and negative 2 SD shapes. Distributions not shown did not have any significant differences between their respective groups.

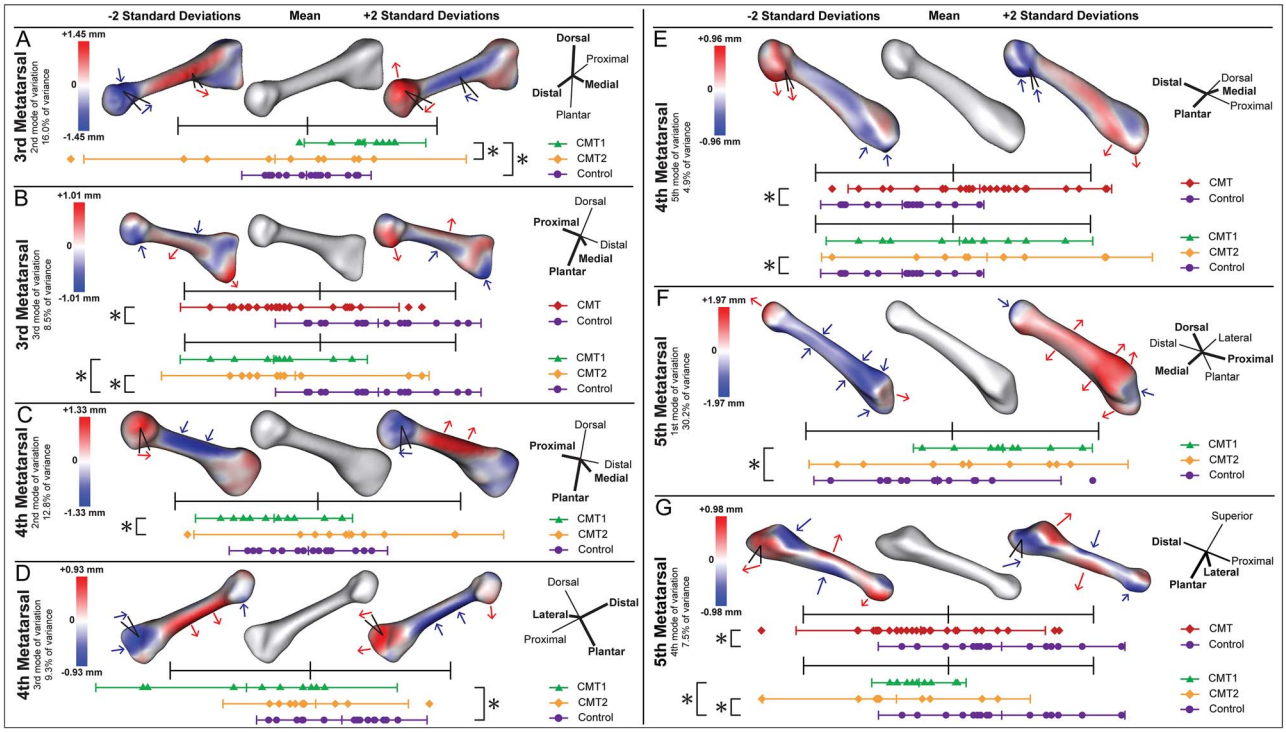

Figure 5. PCA modes in the medial forefoot that had a significant difference between CMT and control groups and/or between CMT1, CMT2, and control groups. These consist of (A) the second mode of variation in the third metatarsal, (B) the third mode of variation in the third metatarsal, (C) the second mode of variation in the fourth metatarsal, (D) the third mode of variation in the fourth metatarsal, (E) the fifth mode of variation in the fourth metatarsal, (F) the first mode of variation in the fifth metatarsal, and (G) the fourth mode of variation in the fifth metatarsal. Red indicates a positive distance from the mean shape and blue indicates a negative distance from the mean shape. Distributions of the CMT and control groups and each of the subtype and control groups are shown underneath the images of the mean, positive 2 SD, and negative 2 SD shapes. Distributions not shown did not have any significant differences between their respective groups.

controls ($p = .027$). The second mode of variation in the third metatarsal (Figure 5A) demonstrated significant differences between the CMT1 group and both the control and CMT2 groups ($p = .003$, $p = .006$). Along this mode, the CMT1 group had increased bending in the axial plane with the metatarsal shaft located more laterally and the head located more medially than in either other group. The third mode of variation in the fourth metatarsal (Figure 5D) demonstrated sagittal plane bending that differed between the CMT1 and control groups ($p = .006$), where the CMT1 group had a more plantar position of the metatarsal shaft as well as a decrease in lateral prominence just distal to the proximal articular surface. Similarly to the first metatarsal, the first mode of variation in the fifth metatarsal (Figure 5F) showed a shorter and thicker fifth metatarsal in the CMT1 group than in either the control or CMT2 groups ($p = .010$, $p = .001$).

Discussion

These data demonstrate bony morphology differences in individuals with CMT throughout the hindfoot, midfoot, and forefoot. Many of the differences seen between CMT1 and CMT2 are attributable to disease severity, where the CMT1 group showed differences to the control and CMT2 groups, which were not significantly different from each other. However, there were several instances where bony morphology differences were present only in CMT2 and minimal cases of differing patterns of morphology variance between subtypes. Unlike previous studies, this analysis did not identify significant morphologic differences between CMT and control groups in the calcaneus.[5] However, a flatter posterior facet and thicker sustentaculum tali were identified in the CMT1 group. The identified flattening of the talus with rotation and thickening of the talar neck, which was more prominent in CMT1 than CMT2, aligns with previous findings of talar morphology differences between CMT1 and CMT2.[7] The decreased bony prominence on the deep transverse fascia insertion of the fibula in CMT1 may be related to altered force along the fascia and interosseous ligaments based on the degree of varus rotation in the hindfoot.

The shorter and narrower navicular tuberosity that was seen in the CMT and CMT1 groups likely corresponds with the more lateral position of the talar head in a cavovarus foot.[38] Increased bone deposition in the inferior medial border of the navicular in CMT1 aligns with the attachment site of the tibialis posterior. The shortening of the cuboid in CMT1 and increased medial-lateral width of the distal articular surface in CMT and CMT2 can be explained by the increased lateral weight-bearing in a cavovarus foot. Morphologic changes in the metatarsals were most evident on the plantar aspects, with decreased bone deposition in the plantar-proximal medial cuneiform and planar intermediate cuneiform and increased bone deposition on the plantar-distal lateral cuneiform. These align with the attachment sites of the plantar Lisfranc ligament and plantar intercuneiform ligament. Proximal-lateral rotation of the intercuneiform articular surfaces of the intermediate cuneiform in CMT2 compared to a medial-distal rotation in CMT1 show a different pattern of morphology variation between subtypes. Taken together,

this variation in the morphology of intercuneiform articulations and ligamentous attachments suggests a difference in the pattern of load distribution through the transverse arch in CMT as compared to controls and between disease subtypes. While some of this variation in shape may be directly related to the severity of cavovarus deformity, the differing patterns of variation may be related to the impact of different disease subtypes on musculotendinous units that insert on the midfoot, different adaptations in gait based on disease subtype, or variation in the bone remodeling response.

In the lateral mid and forefoot, differences were seen in the cuboid and fifth metatarsal between CMT and control groups and between at least 1 CMT subtype and the control group. The primary difference at the fifth tarsometatarsal joint is an increased plantar prominence of the fifth metatarsal and increase in the medial-lateral width of the distal articular surface of the cuboid. However, the interpretation of these results in the context of the whole foot coordinate system is limited because of the extensive varus rotation seen in CMT. Incorporating the impact of this rotation at the whole foot level, the increase in medial-lateral width and superior-lateral protrusion of the articulating surfaces of the 2 bones more accurately represent an increased width along a plantar-lateral to superior-medial direction in the cuboid and an increased plantar-lateral protrusion of the fifth metatarsal base. Similarly, the bending seen in the fifth metatarsal in the superior direction is more accurately a bend in the lateral direction accounting for the varus rotation in CMT. In the other metatarsals, the decrease in sagittal plane bending is surprising, in that a higher arch would seem to necessitate increased sagittal plane bending in order for the metatarsal heads to contact the ground. However, these results indicate a decrease in sagittal bend, suggesting that the forefoot response to the high arch in CMT may be more caused by a change in the alignment at the tarsometatarsal joints or by the observed morphologic differences in the cuneiforms. Additionally, many of the metatarsal heads showed decreased plantar bony prominence in the CMT or CMT subtype groups compared to controls. Since this model normalizes for size variation, this likely does not represent a global decrease in bone mass due to decreased ambulation but may suggest that gait patterns in CMT send less load through the plantar aspects of the metatarsal-phalangeal joints. This reduction in size of the metatarsal head relative to the metatarsal body may also be observed due to the co-occurrence of hammertoes with CMT-related cavovarus deformity, which alters the range-of-motion and loading of the metatarsal-phalangeal joints. Differences between subtypes in the metatarsals predominantly corresponded with differences between the CMT1 and control groups in a similar direction, suggesting that these may align with an overall increased severity in CMT1.

The osseous morphology differences identified in this study are limited by the sample size and wide age distribution. Unfortunately, the rarity of CMT and frequency of surgical intervention prior to presentation to an academic center limit sample sizes for natural history analysis. This study used data from multiple institutions to establish a sample size comparable to previous studies on CMT bony anatomy, which range between 16 and 30 individuals with CMT.[3,5,12,38–42] However, since CMT is a rare disease, large multi-site studies are necessary to generate substantial sample sizes, especially within a more limited age range. Additionally, this study was unable to analyze potential sex-based differences because the available data had significant differences in age and in genetic subtype between sexes that would confound the results and the difference in BMI between groups may also confound these results due to differences in bone loading. This study could only do a small analysis of CMT types 1 and 2 and no analysis of rarer disease subtypes. Because this retrospective data consisted of individuals who had seen foot and ankle surgeons, it is possible that these represent more severe foot manifestations of CMT than the overall population with the disease. However, the pre-operative inclusion criteria may exclude some of the most severe cases, who may have received surgery at other centers prior to presenting to either of the hospitals included in this study. Better characterization of specific disease subtypes and the full spectrum of CMT-related foot deformity requires large, multi-site studies that can generate sufficient data about this rare disease.

The observation of structural differences of bone in CMT challenges the concept of the CMT-related cavovarus deformity as a malignment of the foot and raises an obvious question about the mechanism of osseous morphology change. Bone remodeling is highly responsive to alterations in mechanical stress.[27,43,44] Thus, building from the view of CMT-related foot deformity being an alignment change, one potential mechanism of bony deformation is bone remodeling in response altered alignment causing changes in loading forces on the foot. Some of the bony morphology differences identified in this paper supports this mechanism, including the bending of the fifth metatarsal, which may be due to increased loading on the lateral foot due to varus rotation. Additionally, the morphologic changes identified in the tibia and fibula can be explained as a response to alignment change because the cavovarus position puts greater loading through the medial tibia, leading to increased bone deposition in the medial malleolus and variation in the forces in the interosseous ligaments connecting the tibia and fibula, leading to the morphologic variation seen on the opposing surfaces of those bones. Similarly, the alteration in bending of the metatarsal diaphyses may also be related to loading of the midfoot and forefoot during gait.

Another possible mechanism for bone morphology variation in CMT is bone remodeling in response to alterations in the force on bone from musculotendinous units. For example, the inferior-distal aspect of the medial surface of the medial cuneiform, at the insertion of the tibialis anterior, shows decreased prominence in the CMT and CMT1 groups, which aligns with tibialis anterior weakness that is known to occur in CMT.[45] Similarly, the attachment site of the tibialis posterior, which has increased strength relative to the tibialis anterior in CMT, on the inferior-medial aspect of the navicular shows increased prominence in the CMT and CMT1 groups.[1,46,47] However, the peroneus longus, which is paradoxically spared in CMT, demonstrates the opposite.[1] The attachment site of the peroneus longus on the plantar aspect of the first metatarsal base shows decreased, not increased, prominence in the CMT, CMT1, and CMT2 groups as compared to controls.

The instances of bone remodeling that directly oppose the expected change based on typical muscle function suggest that there are additional mechanisms of bone remodeling that overpower the impact of musculotendinous forces in CMT. There is an established relationship between neuromuscular diseases, including CMT, and decreased BMD, as well as an increased risk of non-osteoporotic fracture in individuals with CMT.[6,48] Further, some gene mutations associated with CMT

have been shown to impact cellular differentiation during osteogenesis, suggesting that this relationship may be further complicated during development.[49–54] Our shape modeling results show morphologic variation in the diaphyses of the tibia and metatarsals, but this analysis cannot isolate potential differences in bone size or density because the shape model was normalized for size using a Procrustes algorithm and the imaging did not include calibration phantoms for BMD analysis. The previously observed decrease in BMD in neuromuscular disease may be related to a decreased BDM and/or cortical thickness in individuals with CMT. This effect may be due to decreased ambulation, but that may not be a large enough effect to account for all the observed differences in osseous morphology. Impact of innervation on skeletal remodeling may play a role in these bony morphology differences. Both sensory nerves and sympathetic nerves have been shown to impact osteoclast numbers, osteoblast activity, stem cell differentiation, and angiogenesis during bone remodeling.[26,55,56] Additional research is needed to describe the influence of impaired innervation secondary to CMT on bone remodeling and on development of the cavovarus foot deformity. Understanding this connection may provide valuable insight into the mechanism of CMT-related foot deformity and may be applicable more broadly to understanding neuro-skeletal interactions in a variety of neurologic and musculoskeletal diseases.[57]

Author contributions

Melissa R. Requist: Study design, image data collection, segmentation, model generation, data analysis, statistical analysis, and manuscript editing.
Andrew C. Peterson: Image data collection, segmentation, MATLAB coding, and manuscript writing.
Timothy C. Beals: Image data collection, manuscript editing, and clinical insight.
Bopha Chrea: Image data collection, manuscript editing, clinical insight, and manuscript writing.
Amy L. Lenz: Study design, grant applications, and manuscript writing.

Supplementary material

Supplementary material is available at *JBMR Plus* online.

Funding

The author(s) disclosed receipt of the following financial support for the research, authorship, and/or publication of this article: Funding was provided by the University of Utah VPR Seed Grant, University of Utah Pediatric Orthopaedic Foundation Grant, and National Institutes of Health (NIAMS, K01AR080221).

Conflicts of interest

None declared.

Data availability

Computational models are available upon request.

References

1. Beals TC, Nickisch F. Charcot-Marie-Tooth disease and the cavovarus foot. *Foot Ankle Clin*. 2008;13(2):259-274vi-vii. https://doi.org/10.1016/j.fcl.2008.02.004
2. Laura M, Singh D, Ramdharry G, et al. Prevalence and orthopedic management of foot and ankle deformities in Charcot-Marie-Tooth disease. *Muscle Nerve*. 2018;57(2):255-259. https://doi.org/10.1002/mus.25724
3. Bernasconi A, Cooper L, Lyle S, et al. Pes cavovarus in Charcot-Marie-Tooth compared to the idiopathic cavovarus foot: a preliminary weightbearing CT analysis. *Foot Ankle Surg*. 2021;27(2):186-195. https://doi.org/10.1016/j.fas.2020.04.004
4. Pareyson D, Marchesi C. Diagnosis, natural history, and management of Charcot-Marie-Tooth disease. *Lancet Neurol*. 2009;8(7):654-667. https://doi.org/10.1016/S1474-4422(09)70110-3
5. Michalski MP, An TW, Haupt ET, Yeshoua B, Salo J, Pfeffer G. Abnormal bone morphology in Charcot-Marie-Tooth disease. *Foot Ankle Int*. 2022;43(4):576-581. https://doi.org/10.1177/10711007211055460
6. Abdala R, Levi L, Longobardi V, Zanchetta MB. Severe bone microarchitecture deterioration in a family with hereditary neuropathy: evidence of the key role of the mechanostat. *Osteoporos Int*. 2020;31(12):2477-2480. https://doi.org/10.1007/s00198-020-05674-9
7. Peterson AC, Requist MR, Benna JC, et al. Talar morphology of Charcot-Marie-Tooth patients with cavovarus feet. *Foot Ankle Int*. 2025;46(3):268-274. https://doi.org/10.1177/10711007241309915
8. An TW, Michalski M, Jansson K, Pfeffer G. Comparison of lateralizing calcaneal osteotomies for varus hindfoot correction. *Foot Ankle Int*. 2018;39(10):1229-1236. https://doi.org/10.1177/1071100718781572
9. Pfeffer GB, Gonzalez T, Brodsky J, et al. A consensus statement on the surgical treatment of Charcot-Marie-Tooth disease. *Foot Ankle Int*. 2020;41(7):870-880. https://doi.org/10.1177/1071100720922220
10. Pfeffer GB, Haupt ET. The surgical correction of cavovarus deformity in Charcot-Marie-Tooth disease. *J Am Acad Orthop Surg*. 2023;31(21):e930-e939. https://doi.org/10.5435/JAAOS-D-23-00056
11. Pfeffer GB, Michalski MP. Charcot-Marie-Tooth disease: a surgical algorithm. *Foot Ankle Clin*. 2023;28(4):857-871. https://doi.org/10.1016/j.fcl.2023.05.005
12. Michalski MP, Blough CL, Song JH, Pfeffer GB. Meary's angle decoded: 3D analysis of first ray plantarflexion deformity in Charcot-Marie-Tooth disease. *Foot Ankle Surg*. 2024;31(2):143-147. https://doi.org/10.1016/j.fas.2024.08.003
13. Lenz AL, Lisonbee RJ. Biomechanical insights afforded by shape modeling in the foot and ankle. *Foot Ankle Clin*. 2023;28(1):63-76. https://doi.org/10.1016/j.fcl.2022.11.001
14. Lenz AL, Krahenbuhl N, Peterson AC, et al. Statistical shape modeling of the talocrural joint using a hybrid multi-articulation joint approach. *Sci Rep*. 2021;11(1):7314. https://doi.org/10.1038/s41598-021-86567-7
15. Peterson AC, Lisonbee RJ, Krahenbuhl N, et al. Multi-level multi-domain statistical shape model of the subtalar, talonavicular, and calcaneocuboid joints. *Front Bioeng Biotechnol*. 2022;10:1056536. https://doi.org/10.3389/fbioe.2022.1056536
16. Requist MR, Mills MK, Carroll KL, Lenz AL. Quantitative skeletal imaging and image-based modeling in pediatric orthopaedics. *Curr Osteoporos Rep*. 2024;22(1):44-55. https://doi.org/10.1007/s11914-023-00845-z
17. Baker-LePain JC, Luker KR, Lynch JA, Parimi N, Nevitt MC, Lane NE. Active shape modeling of the hip in the prediction of incident hip fracture. *J Bone Miner Res*. 2011;26(3):468-474. https://doi.org/10.1002/jbmr.254
18. Bredbenner TL, Mason RL, Havill LM, Orwoll ES, Nicolella DP, Osteoporotic Fractures in Men (MrOS) Study. Fracture risk predictions based on statistical shape and density modeling of the proximal femur. *J Bone Miner Res*. 2014;29(9):2090-2100. https://doi.org/10.1002/jbmr.2241
19. Nelson AE, Golightly YM, Lateef S, et al. Cross-sectional associations between variations in ankle shape by statistical shape

modeling, injury history, and race: the Johnston County Osteoarthritis Project. *J Foot Ankle Res*. 2017;10:34. https://doi.org/10.1186/s13047-017-0216-3
20. Peiffer M, Burssens A, De Mits S, et al. Statistical shape model-based tibiofibular assessment of syndesmotic ankle lesions using weight-bearing CT. *J Orthop Res*. 2022;40(12):2873-2884. https://doi.org/10.1002/jor.25318
21. Fallon, Verbruggen F, Killen BA, Burssens A, Boey H, Vander Sloten J, Jonkers I. Unique shape variations of hind and midfoot bones in flatfoot subjects-a statistical shape modeling approach. *Clin Anat*. 2022;36(6):848-857. https://doi.org/10.1002/ca.23969
22. Gabrielli AS, Gale T, Hogan M, Anderst W. Bilateral symmetry, sex differences, and primary shape factors in ankle and hindfoot bone morphology. *Foot Ankle Orthop*. 2020;5(1):2473011420908796. https://doi.org/10.1177/2473011420908796
23. Lisonbee RJ, Peterson AC, Mills MK, Anderson AE, Lenz AL. Dynamic subtalar joint space measurement analysis following tibiotalar arthrodesis and total ankle replacement. *Clin Biomech (Bristol)*. 2025;123:106464. https://doi.org/10.1016/j.clinbiomech.2025.106464
24. Grant TM, Diamond LE, Pizzolato C, et al. Development and validation of statistical shape models of the primary functional bone segments of the foot. *PeerJ*. 2020;8:e8397. https://doi.org/10.7717/peerj.8397
25. Warden SJ, Galley MR, Hurd AL, et al. Cortical and trabecular bone benefits of mechanical loading are maintained long term in mice independent of ovariectomy. *J Bone Miner Res*. 2014;29(5):1131-1140. https://doi.org/10.1002/jbmr.2143
26. Qin Q, Lee S, Patel N, et al. Neurovascular coupling in bone regeneration. *Exp Mol Med*. 2022;54(11):1844-1849. https://doi.org/10.1038/s12276-022-00899-6
27. Barak MM. Cortical and trabecular bone modeling and implications for bone functional adaptation in the mammalian tibia. *Bioengineering (Basel)*. 2024;11(5):514. https://doi.org/10.3390/bioengineering11050514
28. Reznikov N, Phillips C, Cooke M, Garbout A, Ahmed F, Stevens MM. Functional adaptation of the calcaneus in historical foot binding. *J Bone Miner Res*. 2017;32(9):1915-1925. https://doi.org/10.1002/jbmr.3185
29. Goodall C. Procrustes methods in the statistical analysis of shape. *J R Stat Soc Ser B Methodol*. 1991;53:285-339.
30. Gower J. Generalized procrustes analysis. *Psychometrika*. 1975;40:33-51.
31. Krahenbuhl N, Lenz AL, Lisonbee RJ, et al. Morphologic analysis of the subtalar joint using statistical shape modeling. *J Orthop Res*. 2020;38(12):2625-2633. https://doi.org/10.1002/jor.24831
32. Bin Ghouth SG, Williams SA, Reid SL, Besier TF, Handsfield GG. A statistical shape model of soleus muscle morphology in spastic cerebral palsy. *Sci Rep*. 2022;12(1):7711. https://doi.org/10.1038/s41598-022-11611-z
33. Feng Y, Bishop A, Farley D, et al. Statistical shape modelling to analyse the talus in paediatric clubfoot. *Proc Inst Mech Eng H*. 2021;235(8):849-860. https://doi.org/10.1177/09544119211012115
34. Horn JL. A rationale and test for the number of factors in factor analysis. *Psychometrika*. 1965;30:179-185. https://doi.org/10.1007/BF02289447
35. Borenstein M, Hedges LV, Higgins JPT, Rothstein HR. *Introduction to Meta-Analysis*. West Sussex, United Kingdom: John Wiley & Sons; 2011.
36. Durlak JA. How to select, calculate, and interpret effect sizes. *J Pediatr Psychol*. 2009;34(9):917-928. https://doi.org/10.1093/jpepsy/jsp004
37. Sarrafian SK. *Sarrafian's Anatomy of the Foot and Ankle*. Third Edition ed. Philadelpia, PA: Wolters Kluwer; 2011.
38. An T, Haupt E, Michalski M, Salo J, Pfeffer G. Cavovarus with a twist: midfoot coronal and axial plane rotational deformity in Charcot-Marie-Tooth disease. *Foot Ankle Int*. 2022;43(5):676-682. https://doi.org/10.1177/10711007211064600
39. Ranjit S, Sangoi D, Cullen N, Patel S, Welck M, Malhotra K. Assessing the coronal plane deformity in Charcot-Marie-Tooth cavovarus feet using automated 3D measurements. *Foot Ankle Surg*. 2023;29(7):511-517. https://doi.org/10.1016/j.fas.2023.02.013
40. Sangoi D, Ranjit S, Bernasconi A, et al. 2D manual vs 3D automated assessment of alignment in normal and Charcot-Marie-Tooth cavovarus feet using weightbearing CT. *Foot Ankle Int*. 2022;43(7):973-982. https://doi.org/10.1177/10711007221084308
41. Song JH, Michalski MP, Pfeffer GB. 3D analysis of joint-sparing Charcot-Marie-Tooth surgery effect on initial standing foot alignment. *Foot Ankle Int*. 2024;45(6):601-611. https://doi.org/10.1177/10711007241232976
42. Malhotra K, Patel S, Cullen N, Welck M. Forefoot morphotypes in cavovarus feet: a novel assessment of deformity. *Foot Ankle Int*. 2024;45(7):746-756. https://doi.org/10.1177/10711007241242779
43. Barak MM, Lieberman DE, Hublin JJ. A Wolff in sheep's clothing: trabecular bone adaptation in response to changes in joint loading orientation. *Bone*. 2011;49(6):1141-1151. https://doi.org/10.1016/j.bone.2011.08.020
44. Frost HM. Wolff's law and bone's structural adaptations to mechanical usage: an overview for clinicians. *Angle Orthod*. 1994;64(3):175-188. https://doi.org/10.1043/0003-3219(1994)064<0175:WLABSA>2.0.CO;2
45. Dreher T, Wolf SI, Heitzmann D, Fremd C, Klotz MC, Wenz W. Tibialis posterior tendon transfer corrects the foot drop component of cavovarus foot deformity in Charcot-Marie-Tooth disease. *J Bone Joint Surg Am*. 2014;96(6):456-462. https://doi.org/10.2106/JBJS.L.01749
46. Mann RA, Missirian J. Pathophysiology of Charcot-Marie-Tooth disease. *Clin Orthop Relat Res*. 1988;234:221-228.
47. Seaman TJ, Ball TA. *Pes Cavus*. Treasure Island, FL: StatPearls; 2024.
48. Pouwels S, de Boer A, Leufkens HG, Weber WE, Cooper C, de Vries F. Risk of fracture in patients with Charcot-Marie-Tooth disease. *Muscle Nerve*. 2014;50(6):919-924. https://doi.org/10.1002/mus.24240
49. Zarei A, Ballard A, Cox L, et al. Osteolineage depletion of mitofusin2 enhances cortical bone formation in female mice. *Bone*. 2021;148:115941. https://doi.org/10.1016/j.bone.2021.115941
50. Esseltine JL, Shao Q, Brooks C, et al. Connexin43 mutant patient-derived induced pluripotent stem cells exhibit altered differentiation potential. *J Bone Miner Res*. 2017;32(6):1368-1385. https://doi.org/10.1002/jbmr.3098
51. Akter R, Rivas D, Geneau G, Drissi H, Duque G. Effect of Lamin A/C knockdown on osteoblast differentiation and function. *J Bone Miner Res*. 2009;24(2):283-293. https://doi.org/10.1359/jbmr.081010
52. Masuyama R, Mizuno A, Komori H, et al. Calcium/calmodulin-signaling supports TRPV4 activation in osteoclasts and regulates bone mass. *J Bone Miner Res*. 2012;27(8):1708-1721. https://doi.org/10.1002/jbmr.1629
53. Nuzzo S, Meneghini C, Braillon P, Bouvier R, Mobilio S, Peyrin F. Microarchitectural and physical changes during fetal growth in human vertebral bone. *J Bone Miner Res*. 2003;18(4):760-768. https://doi.org/10.1359/jbmr.2003.18.4.760
54. Sabag E, Halperin E, Liron T, Hiram-Bab S, Frenkel B, Gabet Y. Hormone-independent sexual dimorphism in the regulation of bone resorption by Krox20. *J Bone Miner Res*. 2019;34(12):2277-2286. https://doi.org/10.1002/jbmr.3847
55. Chen H, Hu B, Lv X, et al. Prostaglandin E2 mediates sensory nerve regulation of bone homeostasis. *Nat Commun*. 2019;10(1):181. https://doi.org/10.1038/s41467-018-08097-7
56. Chenu C. Role of innervation in the control of bone remodeling. *J Musculoskelet Neuronal Interact*. 2004;4(2):132-134.
57. Tosi LL, Warman ML. Mechanistic and therapeutic insights gained from studying rare skeletal diseases. *Bone*. 2015;76:67-75. https://doi.org/10.1016/j.bone.2015.03.016

JBMR Plus, 2025, 9, ziaf058
https://doi.org/10.1093/jbmrpl/ziaf058
Research Article